Theoretical Findings and Measurements on Planning a UHF RFID System inside a Room

Antonis G. DIMITRIOU[1], Aggelos BLETSAS[2], Anastasis C. POLYCARPOU[3], John N. SAHALOS[3]

[1]Dept. of El. & Computer Engg., Aristotle Univ. of Thessaloniki, AUTh Campus, ECE Dept., 54124 Thessaloniki, Greece
[2]Dept. of Electronic & Computer Engineering, Tech. Univ. of Crete, TUC Campus, Kounoupidiana, 73100 Chania, Greece
[3]Department of Electrical & Computer Engineering, University of Nicosia, Makedonitissas Ave. 46, 1700 Nicosia, Cyprus

antodimi@auth.gr, aggelos@telecom.tuc.gr, polycarpou.a@unic.ac.cy, sahalos@auth.gr

Abstract. *This paper investigates the problem of improving the identification performance of a UHF RFID system inside a room. We assume static reader, passive tags and availability of commodity antennas. A ray-tracing propagation model is developed that includes multipath in 3D space. It is found that careful selection of reader antenna placement and tilting must be performed to control destructive interference effects. Furthermore, 3D coverage performance gains on the order of 10% are observed by implementing tags' diversity. A device that successfully manipulates destructive interference is introduced. All theoretical findings are verified by measurements. Finally, a method to perform propagation measurements with commodity RFID hardware is demonstrated.*

Keywords

Radio frequency identification, planning, UHF, tags, diversity.

1. Introduction

Radio Frequency Identification (RFID) is widely adopted, replacing traditional barcode applications in supply chain management while initiating numerous range-demanding applications (e.g. books' tracking in libraries, luggage tracking in airports, or even high-values chips in casinos). RFID's future-success depends on decreasing the cost of equipment (tags, readers, antennas) and increasing the reliability of such installations. UHF RFID systems have extended the identification-range of the original LF or HF RFID systems. Depending on the type of tags implemented, a UHF EPC Gen2 operating RFID reader can identify "passive" tags within a few meters or "active" tags within tens of meters.

Read-region is usually defined by approximate or stochastic models [1] - [5]. Propagation was analyzed stochastically in [2], where multipath was modeled by a suitable Ricean or Rayleigh distribution. Hence, the probability for successful identification of a tag can be evaluated. A stochastic model, suitable for multiple reader and tag antennas was presented in [4], where diversity gains were investigated by utilizing multiple tags.

The model in [5] evaluates a "reliable" reading region in the presence of multipath and is suitable for single-lobe directional antennas. The minimum resulting field of a two-ray model, composed of the direct ray and a ray reflected from the closest wall in the direction of reader's antenna maximum gain, was approximated. The read-region was approximated by an ellipsoid, including reader-antenna's location, while its axes depend on the half-power beamwidth of the antenna. The validity of the proposed model in [5] depends on the location and the direction of the reader's antenna with respect to the surrounding walls; the basic assumption is that the direct field interacts with a single reflector. However, the model would fail if two or more antennas were fed via a splitter, as the resulting field, due to the interaction of the two antennas, is complex and the corresponding coverage region is not continuous even at the vicinity of the antennas, as demonstrated later in this work.

The problem of planning an operational RFID network of readers in a specific environment has been overlooked. In this paper, we treat the problem of maximizing the coverage of a UHF RFID system operating inside a single room with commodity RFID hardware. This represents part of a greater project that includes the design and implementation of a pilot RFID system inside a hospital [6]. Passive tags are attached to medical equipment, such as infusion pumps and wheelchairs inside a room. Our goal is to maximize the identification percentage within a given volume of interest, as demonstrated in Fig. 1.

We developed a ray-tracing model, capable of including the complex environment in the estimation process. The field inside the volume of interest is calculated as the superposition of several contributions arriving from diverse propagation paths. The radiation pattern and the polarization of the reader's antennas as well as the tags' antennas, the frequency of operation, the constitutive parameters of the walls and the transmission power are considered. Conclusions are derived on antenna selection, antenna placement and orientation, tags' diversity. Finally,

we propose the introduction of a switch-controlled phase shifter in the feeding of double antenna configurations, capable of minimizing destructive-interference effects and thus, boosting coverage performance and system reliability.

All theoretical findings are verified by measurements that were conducted in a "controlled" environment in Thessaloniki, Greece and then under "operational" conditions in a hospital-room in Nicosia, Cyprus.

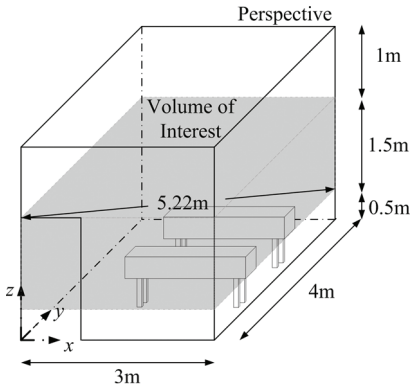

Fig. 1. Room representation with volume of interest.

2. Propagation Model

A ray-tracing model [7] that includes the direct and the multiply reflected fields at each location was developed. Proper algorithms for the manipulation of vectors and their transformations among different Spherical and Cartesian coordinate systems have been realised.

For a linearly polarized antenna, the magnitude of the radiated far-zone electric field component E_{inc} at distance r is:

$$E_{inc} = \sqrt{\frac{\eta P_t G_t(\theta,\phi)}{2\pi}}\frac{1}{r}. \tag{1}$$

P_t is the transmission power in Watts, $G_t(\theta,\varphi)$ is the antenna's gain at angles θ, φ and η is the free-space intrinsic impedance. In order to model a circularly polarized antenna, another vector field component, orthogonal to the above and with a $\pi/2$ phase delay, along with its corresponding radiation pattern is considered.

For each reflection, the incident field on the boundaries of a wall is analyzed in two orthogonal vectors; one parallel to the plane of incidence and one perpendicular. Then, the reflection coefficients are calculated by employing the recursive formulation presented in [8]. A uniform plane wave incident at an oblique angle upon N layers of planar dielectric slabs that are bordered on either side by free space is considered. The constitutive parameters of the wall are taken into account by selecting the permittivity and the loss tangent of each layer [9], [10]. Each reflection might lead to a different phase shift and magnitude-change of the vertically and the horizontally polarized components of the incident field respectively, thus leading to a change in the polarization state of the reflected field with respect to that of the incident field.

Each ray is traced until it reaches the receiver's position. At the receiver, the field from each path is decomposed in three orthogonally arranged axes x, y, z. Assuming that the electric field component of the i^{th} ray along the tag's polarization axis is E_i^{tag}, the total field at the tag's antenna is given as the phase sum of all contributions:

$$E^{tag} = \sum_{i=1}^{N}\sqrt{G^{tag}\left(\theta_i^{tag},\phi_i^{tag}\right)}E_i^{tag}e^{j(2\pi ft+2\pi r_i/\lambda+\varphi_i)} \tag{2}$$

where r_i is the distance traveled by the i^{th} ray and φ_i is the phase shift of the specific contribution, due to the reflections on the surrounding walls, $G^{tag}(\theta_i^{tag},\phi_i^{tag})$ is the gain of the tag's antenna at the angle-of-arrival $\theta_i^{tag},\phi_i^{tag}$ measured at a spherical coordinate system centered at the tag and λ is the wavelength of operation.

Finally, the power at the tag's chip P_{tag} is given as:

$$P_{tag} = \frac{\lambda^2}{4\pi}\frac{E_{tag}^2}{2\eta}\tau \tag{3}$$

where τ is the power transmission coefficient, expressing mismatches between the chip's impedance $Z_c = R_c + jX_c$ and the antenna's impedance $Z_a = R_a + jX_a$:

$$\tau = \frac{4R_cR_a}{\left|Z_c+Z_a\right|^2},\quad 0\le\tau\le 1. \tag{4}$$

Such detailed model represents the foundation for accurate characterization of the multipath profile and allows the development of techniques that control interference effects, as will be demonstrated later.

3. Definition of Coverage

Literally, a point in space is considered covered, if the modulated backscattered field (from a passive tag at that point) reaches the reader with sufficient power, i.e. with power above reader's sensitivity threshold. In the case of passive UHF RFID tags, as examined herein, the radiated power from the reader's antenna is needed to power up the tag's IC that employs a rectifier circuit [11]. Typically, tag-to-reader communication is binary modulated, with conjugate match of tag's antenna to the IC chip in the first state and optimized tag's design in the second state [12]; if the incident power is sufficient to power up the tag's IC, then the back-scattered power at the reader is typically much greater than its sensitivity level [13]. Therefore, identification is accomplished if the tag is powered up and coverage in this work depends on the required minimum power to activate tag's chip. This quantity is calculated in (3).

The corresponding measured power sensitivity of two major UHF Gen2 RFID chips varied between -11.5 dBm and -12.5 dBm [13]. Significantly improved sensitivity values have been reported recently by major manufacturers, ranging from -15 dBm [14], [15] down to -18 dBm [16]. However, it must be emphasized that the nominal threshold may not be accomplished in the entire operating frequency band, due to the variation of the tag IC impedance with frequency. Also, depending on the material where the tag is attached to, one should expect a gain loss [17] ranging from 1 dB (for paper or acrylic) up to more than 10 dBs for aluminum surfaces, where specialized tags need to be designed.

It is desired not to restrict the analysis in the following sections to a specific tag, but to include important parameters of the problem, like polarization. We calculate the received power, using the analytical ray-tracing model described in (1) - (4), along three orthogonally arranged axes x, y, z, thus taking into account the polarization of the incident field with respect to that of the tag's antenna, on the tips of a cubic grid. The radiation pattern of the tag's antenna is considered omni-directional with 0 dBi gain, in order not to favor specific directions-of-arrival of the different field components; the transmission coefficient τ is assumed equal to 1. A tag is considered "identified" if the power at the polarization axis of the tag is greater than the tag's sensitivity threshold.

Thus, for a given tag's sensitivity threshold, we can estimate the coverage percentage, or identification percentage, in any area or volume of interest and for any polarization of the tag's antenna, including circular polarization or polarization-diversity by evaluating the ratio of the points identified N_{id} over the total number of grid-points N_{tot}: N_{id} / N_{tot}. Some representative results are given in Fig. 4, for a z-polarized tag at three different heights inside the room as well as in the entire volume of interest (Fig. 1). The tag's sensitivity threshold is varied from -14 dBm up to -4 dBm. These results are presented in the following section.

4. Estimation Results

The target is to maximize the coverage percentage within a volume of interest inside a room, as demonstrated in Fig. 1. The available antennas are manufactured by "MTI Wireless" [20]. The tags are expected to be both horizontally as well as vertically attached to the objects of interest, depending on geometry of the latter. In order to transmit power polarized along the horizontal and the vertical plane, circularly polarized transmitting antennas have been selected. One is the "MT-242017/NRH" with 10 dBic gain and dimensions equal to 37 cm × 37 cm (3 dB beamwidth: 60° azimuth, 48° elevation) and the other is the "MT-242032/NRH" with 7 dBic gain and dimensions 19 cm × 19 cm (3 dB beamwidth: 72° azimuth, 73° elevation).

Initially, some characteristic results are demonstrated. The "MT-242017/NRH" antenna is considered at the position shown in Fig. 2, properly tilted, so as to illuminate the volume of interest. The transmission power is set to 30 dBm at the frequency of 865 MHz. The vertical walls and the ceiling are modeled as reinforced concrete walls [9] with $\varepsilon_r = 6.5$ and $\tan\delta = 0.287$. The floor is modeled as "wet ground" with $\varepsilon_r = 30$ and $\tan\delta = 0.103$ [10]. The power is calculated in the entire room at the nodes of a cubic grid spaced by 10 cm. The received power along a constant x-plane (Fig. 2) at $x = 2.5$ m for a z polarized tag is given in Fig. 3. Similar results can be extracted for any polarization axis and for any cut. By combining these results, one can recognize the dominant propagation mechanisms that are responsible for the field's interference patterns inside the room due to multipath and then properly move the antenna inside the room, manipulating the resulting field as desired.

As discussed in the previous section, coverage plots are formed by processing the power results. In Fig. 4, the coverage results for a z polarized tag for increasing tag's threshold are given. Coverage curves are given in three selected heights, at 0.5 m, 1.2 m and 1.8 m above the ground, as well as aggregate results in the entire volume of interest (shown in Fig. 1). Coverage performance is calculated at different heights, as we seek for balanced performance in the entire volume of interest. Similar plots are obtained for all polarization axes.

4.1 Tags' Diversity

In the introduction it was mentioned that asset tracking involves wheelchairs and infusion pumps. Benefiting from the tags' low cost and small dimensions, combined with the tracked-objects' large dimensions, we can associate an object with multiple tags. To examine this case of diversity, we assume three tags polarized in the x, y and z directions respectively, attached to each object. In each location, successful identification is guaranteed if at least one of the tags is powered up. The coverage performance assuming three orthogonally arranged tags at each location is shown in Fig. 5. Aggregate coverage increases by 10 % at the -14 dBm threshold, reaching 89 %, compared to the single z-polarized-tag case shown in Fig. 4. Even better improvement is recorded at greater tag's sensitivity threshold.

4.2 Actual Field vs. Free-Space Estimation

In "Free-Space" (FS) conditions, only the direct path is considered and therefore no multipath interference patterns exist. As a result, the coverage volume is continuous around the reader's antenna and no tag can be identified outside this volume. In real-multipath conditions, the phase-sum of multipath components creates covered-regions even beyond the bounded volume under "FS" conditions (constructive sum), but also introduces "holes"

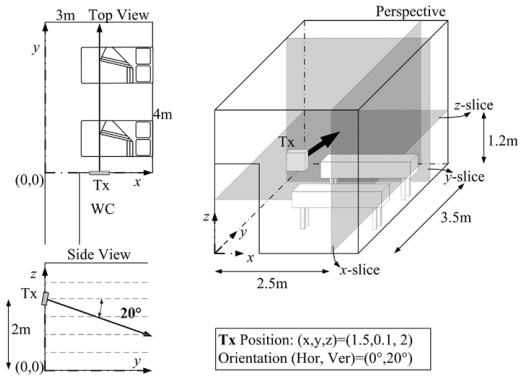

Fig. 2. Representation of a single antenna configuration in top view and side view.

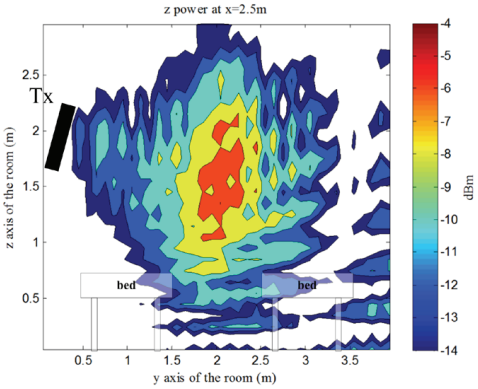

Fig. 3. Received power for a z-polarized tag at x=2.5m.

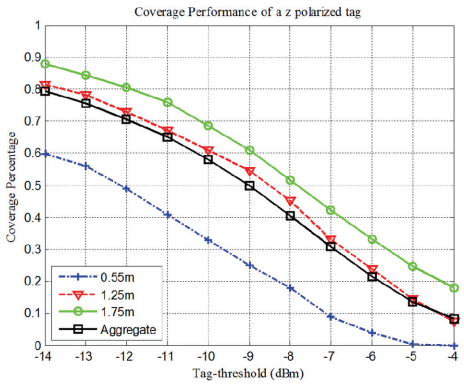

Fig. 4. Coverage percentage of a z-polarized tag for increasing tag's threshold.

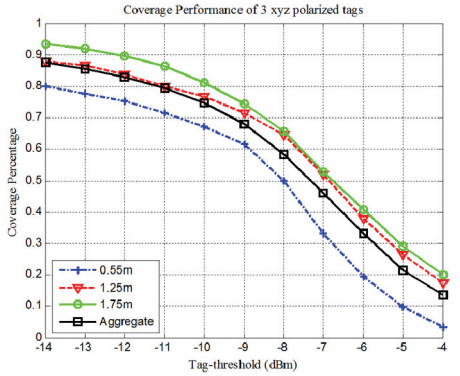

Fig. 5. Coverage percentage, assuming 3 orthogonally polarized tags at each location.

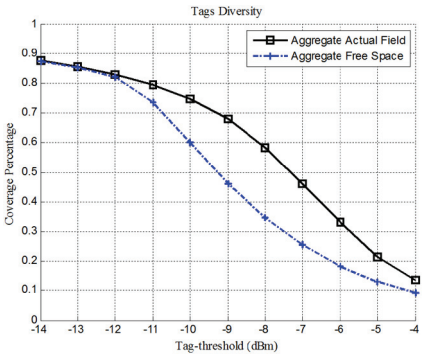

Fig. 6. Coverage performance assuming free space conditions vs. the actual field.

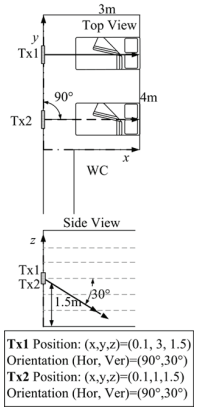

Fig 7. Configuration 1.

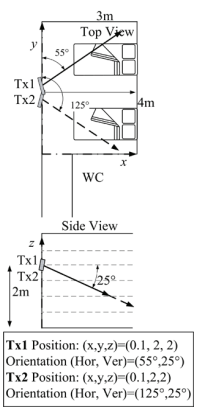

Fig 8. Configuration 2.

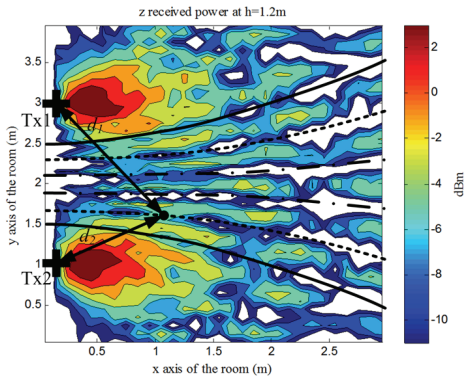

Fig. 9. Received power for a z-polarized tag at z=1.2m for Configuration 1.

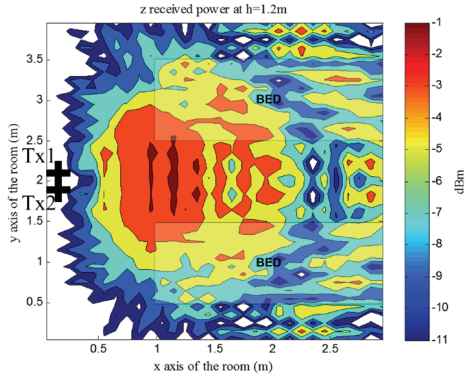

Fig. 10. Received power for a z-polarized tag at z=1.2m for Configuration 2.

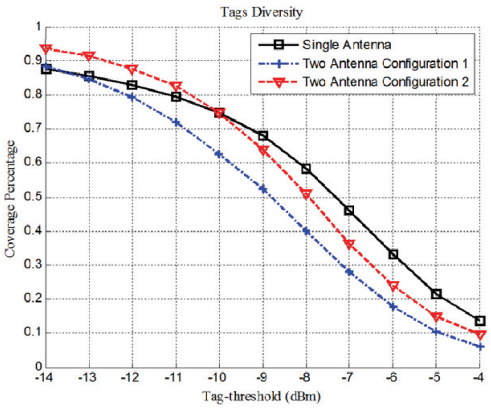

Fig. 11. Coverage performance of the double antenna configurations vs. the single antenna one.

of coverage inside the bounded volume under "FS" conditions (destructive sum). Therefore, one cannot easily predict the percent-coverage under real conditions.

For example, for the same configuration shown in Fig. 2, we calculate the field inside the same volume, assuming free-space conditions. By comparing the coverage performance of the two cases in Fig. 6, assuming tags' polarization diversity as discussed in the previous paragraph, better coverage is accomplished when considering the actual field.

The problem in the real environment, due to multipath, is the reliability of the coverage at any given point. At "free-space" conditions a position is covered depending only on the transmitted power and the radiation pattern of the antenna. In the "real room", coverage depends on the phase and magnitude relations of the different contributions, thus creating "coverage-holes" due to destructive interference even at the vicinity of the antenna. In Section 5, a device is proposed to reduce such effects when multiple antennas are used.

4.3 One vs. Two Reader Antenna Configuration

By considering any of the available transmitting antennas, at several configurations inside the room (different walls, center or corner, different tilting), part of the volume of interest to the left or to the right of the antenna may not be sufficiently covered, due to the narrow 3 dB beamwidth of the horizontal radiation patterns of the two antennas.

To overcome this limitation, five different double antenna configurations were tested. Two of these setups that reveal important properties of the field inside the room are demonstrated in Figs. 7 - 8. The two antennas are fed via a 3 dB bi-directional power splitter/combiner and both transmit the same signal. As a result, each antenna transmits at 3 dB smaller power level (27 dBm) than in the single-antenna configurations. Hence, a fair comparison with the single antenna configurations can be carried out, given that the same amount of power is radiated inside the room. In addition, as the antennas were to be installed inside a patient's room, the "MT-242032/NRH" with 7 dBic gain antennas were selected, due to their significantly reduced dimensions, as compared to the 10 dBic antenna. The EIRP (Effective Isotropic Radiated Power) per antenna and per excitation axis is 31 dBm, which is much smaller than the maximum permissible limit in Europe (3.28 W EIRP).

Fig. 9 shows the power along a constant z-plane at $z = 1.2$m for a z-polarized tag for "Configuration 1" (Fig. 7). The hyperbolas, drawn in Fig. 9, represent the geometric-space of the points in the room with distances from the two sources d_1, d_2 respectively, such that the direct fields from the two antennas contribute with π phase difference, hence add destructively. Depending on the magnitude of each direct contribution, the minimum could be low enough, that a tag at this location is not identified, despite of its small distance from the two antennas. Therefore, in this case, the two antennas form an antenna-array, creating minima at predictable locations.

Therefore, if maximum-coverage is sought, destructive interference-patterns among the antennas should be minimized. One idea is to position the antennas, in close vicinity (distance smaller than $\lambda/2$) and properly rotate them so that they illuminate different parts of the room. These constraints are well satisfied by "Configuration 2" shown in Fig. 8. The two antennas illuminate different parts of the room, so that the 3 dB horizontal beamwidths of each of the antennas radiate at different angular segments. A z-slice at 1.2 m of the z-polarized received power is shown in Fig. 10.

The coverage performance of the two-antenna configurations of Fig. 7 is shown in Fig. 11, assuming tags' diversity. "Configuration 2" ensured 93 % coverage at -14 dBm. By comparing the coverage performance of "Configuration 2" with the corresponding one for the single antenna configuration, shown in Fig. 2, better coverage percentage is accomplished at the expected tags' sensitivity thresholds, as demonstrated in Fig. 11, despite the fact that each of the two antennas radiates at 3 dB smaller power level. The reason is that the transmitted power is better directed towards the volume of interest.

5. Introducing a Phase-Shifter

Despite the fact that 93 % coverage was accomplished with a double antenna configuration, fed via a 3 dB splitter, it was found that the remaining 4 double antenna configurations suffer from destructive interference effects, causing severe degradation of the coverage performance of the system. Directing the power towards the volume of interest is not a sufficient condition for effective planning. Control of destructive-interference effects represents an equally important parameter of the problem. In addition, the expected coverage-performance remains sensitive to possible installation faults.

As discussed earlier, the two antennas behave as an array introducing "holes" in the surrounding area based on the magnitude and phase of the transmitted fields. The desired effect is to "control" the locations of the holes and properly "move" them inside the room.

We propose the selective introduction of a phase-delay in the feeding path of one of the antennas controlled by an electronic switch (Fig. 12). A switch controls feeding of one of the antennas, either with zero phase delay (hence the two antennas radiate in phase) or introducing a π phase delay. Thus in the two states of the switch the "holes" in the room are displaced since destructive interference occurs at different positions inside the room and the coverage performance of the system is boosted. The proposed device can only manipulate destructive interference caused by the destructive sum of contributions from different antennas and not the minima caused due to the field originated by the same antenna (e.g. due to scattering).

In five different configurations, including 3 setups not shown, where coverage was as low as 76 %, identification is increased above 93 % with tags' diversity (Fig. 13). Another important benefit of the introduction of a phase-shifter is that the system can tolerate possible installation faults. The planning rule is simplified to "directing the energy towards the area of interest", while "maintaining some interaction between the two antennas", in order to produce switch-controlled interference patterns.

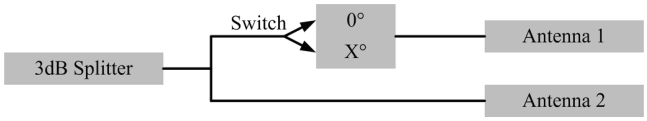

Fig. 12. Introducing a switch controlled phase-shift in the feeding of one antenna.

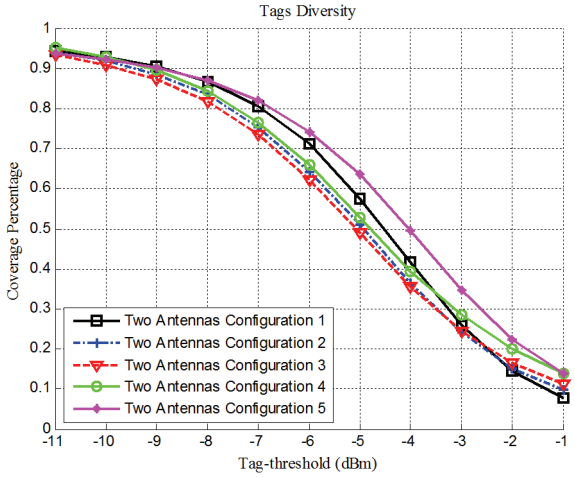

Fig. 13. Coverage performance of the 5 double antenna configurations, after the introduction of the proposed switch-controlled phase shift π.

6. Measurements

Two measurement campaigns were conducted in order to verify the theoretical findings. Initially, measurements were held in a "controlled" environment to verify the theoretical results. The 2nd set of measurements was performed in the hospital-room, under "operational conditions" to evaluate the performance of the system.

6.1 Measurements in "Controlled Environment"

An empty office with dimensions 3.5 m × 3 m in the Department of Physics of the Aristotle University of Thessaloniki was used. 120 "ALN-9662-SH" [18] passive RFID tags were hung by cotton threads in two levels, creating a 3-dimensional measurements' grid, as demonstrated in Figs. 14, 16. At each sample-position of the grid, two tags were suspended side-by-side; one vertically and the other horizontally polarized. The dimensions of the measurements' volume were 2.5 m × 2 m × 0.5 m, as illustrated in Fig. 16; thus, smaller than the target-room's dimensions, shown in Fig. 2.

Five antenna geometries were measured with the 7 dBic and the 10 dBic antennas, resulting in 10 measurements' setups, as shown in Fig. 15. The "Speedway IPJ-R1000" [15] UHF Gen2 RFID tag reader was connected to the transmitting antenna(s) via a single antenna port. A splitter was used for the double-antenna configurations, as shown in Fig. 14. In order to measure the performance of the proposed phase shifter, we selectively introduced a 13 cm long delay in the feeding path of one of the antennas, as demonstrated in Fig. 14. For the expected refractive index of 1.4 (with respect to free space), the delay line introduces a phase shift of 180°. The double antenna measurements were carried out twice: once without the delay line and then with the delay line. The channel can be considered stationary, since the measurements were conducted on Sunday when the building was empty.

For each measurement, the transmitted power was reduced from 30 dBm to 15 dBm in steps of 1 dB at 4 s intervals. For each transmission power level, all 120 installed tags were interrogated. By gradually reducing the transmission power, we recorded the marginal Tx power level, when each of the 120 tags was no longer identified. At this power level, the power at the tag is marginally smaller ($\leq$ 1 dB – the step variation of power) than the sensitivity of the tag. The "ALN-9662-SH" tag is powered by Alien's Higgs 3 UHF RFID IC, which has a nominal "sensitivity during read" threshold of -18 dBm [16]. From the tag's datasheet at 865 MHz, we expect 0.5 dBs losses due to mismatch [18]. Considering 1.5 dB additional losses due to the radiation pattern of the tag's antenna (the measured field is not necessarily at the direction of maximum gain of the tag's antenna), we estimate that the power at the location of the tag when the tag is marginally

identified for the last time equals -16 dBm at the polarization axis of the tag. For a tag that is never identified (even for the maximum Tx power of 30 dBm), we conclude that the received power is less than -16 dBm.

Consider that for a random location i, a tag was ultimately identified when Tx-power was set to P_i dBs. Then the reception level R_i at maximum Tx power P_{max} is:

$$R_i = -16 \text{ dBm} + (P_{max} - P_i). \quad (5)$$

Hence, by exploiting the constant tag's "sensitivity-during-read-threshold", we can create reception power plots inside the room within a dynamic range of 15 dBs and a resolution of 1 dB.

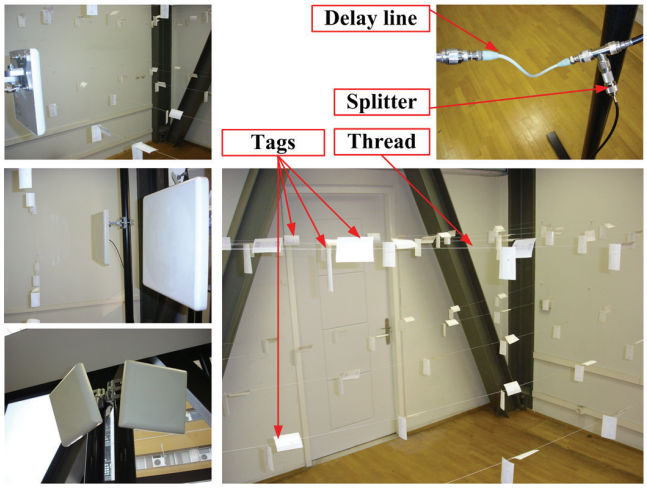

Fig. 14. Photos of the measurements' setup.

In the same time, we derive typical coverage results for the two polarizations for decreasing transmission power level.

A comparison between the theoretical results, when implementing the ray-tracing model and the measurements for "Measurements' Configuration I" (see Fig. 15), is presented in Figs. 17 - 18. The measurements are taken every 50 cm, while the expected field is evaluated every 10 cm. This explains the denser fading recorded by the simulations. The measurements agree reasonably well with the simulations: *a*) the poor reception regions I and II close to the walls to the left and to the right of the antenna are verified, *b*) the strong reception region III due to constructive interference opposite the antenna is also verified, *c*) the strong reception region IV in the vicinity of the antenna is confirmed and *d*) the region V of destructive interference around 2 m from the antenna is partly verified, probably because of down-sampling in the measurements' room.

The coverage performance for the same configuration is demonstrated in Fig. 19. It is verified that tag-polarization diversity enhances coverage performance by approximately 10 %, as suggested in theory.

The benefits by implementing the proposed phase-shifter are illustrated in Figs. 20 - 22. The measured power without and with the phase-shifter for the *x*-polarized field of "Measurements' Configuration IV" at height =1.85 m, are shown in Figs 20 and 21, respectively. Notice that the phase shifter eliminates the "hole" created due to destructive summation of the fields from the two antennas, but cannot eliminate a "hole" due to the environment. The strong metallic scatterers, photographed in Fig. 15, are demonstrated as well at the given *z*-cut, as they represent the probable reason for the introduction of the "hole" (they would create a strong scattered field in their vicinity that interacts with the direct contribution from the antennas). In Fig. 22, the coverage performance when implementing the proposed phase-shifter is demonstrated, yielding an improvement in the order of 10 %.

The coverage performance of the double antenna configurations of Fig. 22 appears worse than that of the single antenna configuration of Fig. 19 because the available power splitter, at the time of the measurements, had an insertion loss of 4 dB (in addition to the 3 dB coupling-loss per antenna). The typical insertion losses for a commercial low-cost quality splitter are less than 0.2 dB [19].

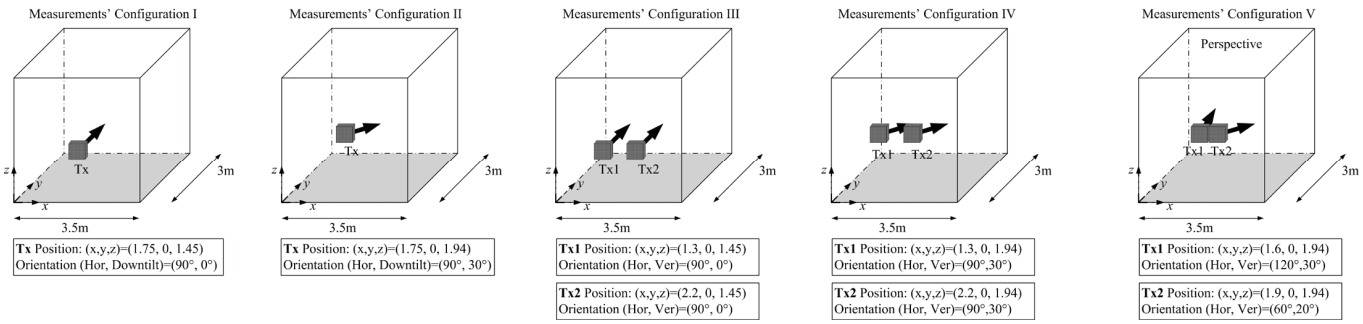

Fig. 15. Measurements' configurations.

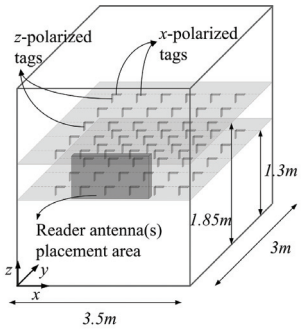

Fig. 16. Measurements' grid.

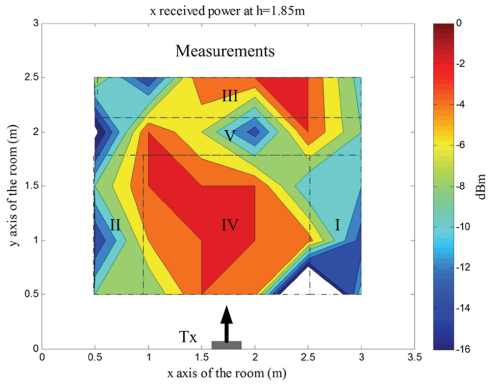

Fig. 17. X-polarized measured field at 1.8 m height for "Measurements' Configuration I".

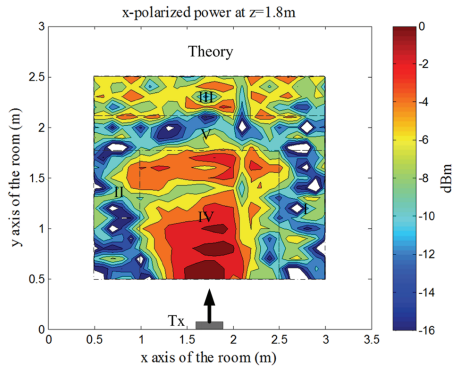

Fig. 18. X-polarized simulated field at 1.8 m height for "Measurements' Configuration I".

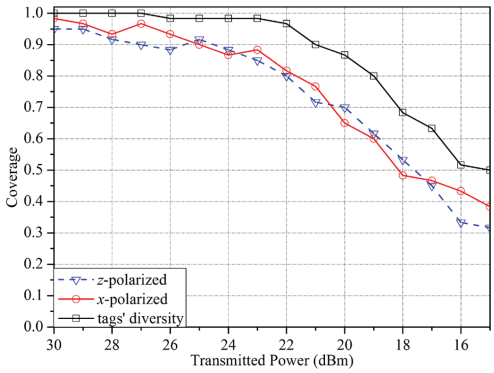

Fig. 19. Measured performance, demonstrating coverage improvements by implementing tags' polarization diversity.

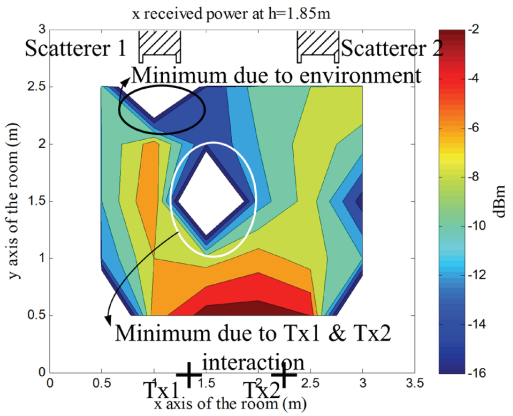

Fig. 20. X-polarized measured field at 1.8 m height for "Measurements' Configuration IV" without the phase shifter.

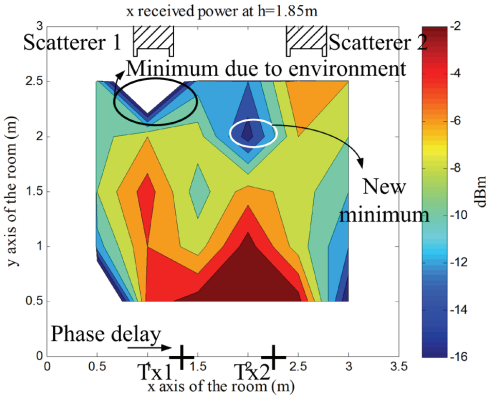

Fig. 21. X-polarized measured field at 1.8 m height for "Measurements' Configuration IV" with the phase shifter.

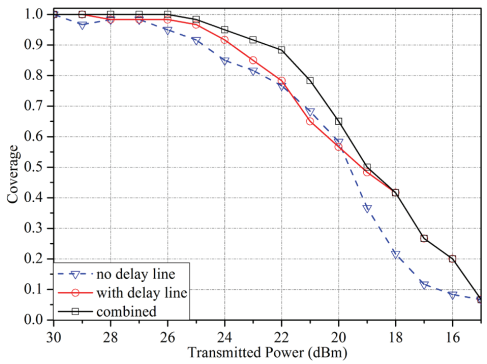

Fig. 22. Measured coverage improvement by implementing the proposed switch controlled phase-shifter.

Fig. 23. 20 tags are attached to a box.

Fig. 24. Antennas positioned in a hospital's room.

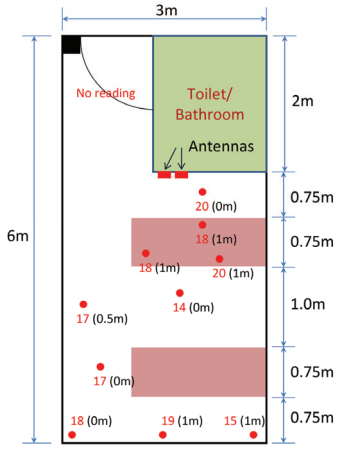

Fig. 25. Vertical polarization.

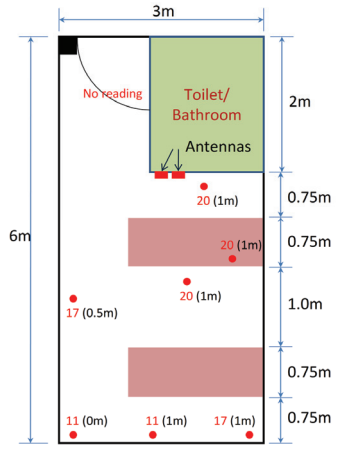

Fig. 26. Horizontal polarization.

6.2 Measurements under Operational Conditions

A number of measurements were conducted at the hospital ward of the Bank of Cyprus Oncology Center in Nicosia in order to assess the overall performance of the installed RFID system. In order to meet the objectives of this experiment, a rectangular cardboard-made box, shown in Fig. 23, was built. A total of 20 "ALN-9662-SH" RFID tags co-aligned along the longest dimension were attached to the box. This box was placed vertically or horizontally at different positions and heights within the room. A 100 % electromagnetic coverage translates to reading and identifying all 20 tags on the box.

The reader [15] has 4 output ports. Each port is connected to an antenna pair, scanning a single room, through a bi-directional power splitter/combiner [19]. As a result, the reader is placed centrally in the hospital ward and 10 m-long low loss cables manufactured by "Andrew" [21], run through the ceiling towards each room. Cable losses were 1.3 dB at the operating frequency, while the splitter inserted additional 0.4 dB losses [19].

The reader was allowed a period of 5 seconds to radiate the room by the two side-by-side "MT-242032/NRH" antennas depicted in Fig. 24. The antennas were mounted at a height of 2 meters from the ground and the measurements were performed when the antennas had no azimuth or elevation tilt angles; in other words, they were faced normal to the wall. The reader transmitted at the maximum power level of 30 dBm; hence 25 dBm were radiated by each antenna, accounting for losses due to cables, connectors and splitter.

The measurements for vertical and horizontal alignment of the box are depicted in Figs. 25 and 26 respectively. The marker (dot) indicates the position of the box, the number in the parenthesis indicates the height of the box, and the number in red indicates how many tags were identified for that particular location.

A total of 88 % coverage is recorded for the vertically polarized tags and 83 % for the horizontally polarized tags. At the target height above 0.5 m the coverage percentage, regardless of the polarization, is 89 % and for the region ≤ 0.5m , this reduces to 81.4 %. This performance is accomplished without polarization diversity or the proposed switch-controlled phase shifter. An even higher coverage could be accomplished, by implementing the proposed techniques.

7. Conclusions

A ray-tracing site specific propagation model has been developed for accurate UHF RFID systems' planning. Coverage optimization inside a single room for a static RFID reader, assuming only passive tags was investigated. The problem has been treated in a 3 dimensional volume. It was shown that tags' polarization diversity can greatly enhance the identification percentage of the system.

Careful reader antenna placement must be performed in order to minimize destructive interference effects caused by the surrounding environment. When several antennas are used, additional interference effects due to the phase-sum of the fields from the antennas are introduced. Destructive interference effects create minima even at the vicinity of the antennas which should be controlled.

For this reason single antenna installations should be preferred, provided that the radiation pattern of the selected antenna can illuminate the target volume adequately. If multiple antennas are needed, they should be placed so that minimum interaction exists among them; a simple rule is to

keep the 3 dB angular segments of the two antennas non-overlapping.

Alternatively, we propose the installation of a switch controlled phase shifter in the feeding of one of the antennas in order to displace the locations of the coverage holes in the two states of the switch, thus increasing the reliability and the coverage performance of the system.

All theoretical findings have been verified by measurements in "controlled" and "operational" conditions. Furthermore, a method to carry out propagation measurements was demonstrated by using commodity RFID hardware. The idea is to gradually reduce the reader's transmitted-power and mark the power level for which a tag fails to be identified, thus exploiting the constant tag's "sensitivity during read" threshold.

Acknowledgements

This work was conducted under the COST ic0603 "Antenna Systems & Sensors for Information Society Technologies" (ASSIST) umbrella and was funded by the Cyprus Research Promotion Foundation grant ΤΠΕ/OPIZO/0308(BIE)/13.

References

[1] GRIFFIN, J. D., DURGIN, G. D. Complete link budgets for backscatter-radio and RFID systems. *IEEE Antennas and Propagation Magazine*, 2009, vol. 51, no.2, p. 11 - 25.

[2] LAZARO, A., GIRBAU. D., SALINAS, D. Radio link budgets for UHF RFID on multipath environments. *IEEE Transactions on Antennas and Propagation*, 2009, vol. 57, no. 4, p. 1241 - 1251.

[3] DOBKIN, D. M. *The RF in RFID: Passive UHF RFID in Practice*. Burlington (MA, USA): Newnes, 2008.

[4] GRIFFIN, J. D., DURGIN, G. D. Gains for RF tags using multiple antennas. *IEEE Transactions on Antennas and Propagation*, 2008, vol. 56, no 2, p. 563 - 570.

[5] MARROCCO, G., DI GIAMPAOLO, E., ALIBERTI, R. Estimation of UHF RFID reading regions in real environments. *IEEE Antennas and Propagation Magazine*, 2009, vol. 51, no 6, p. 44 - 57.

[6] POLYCARPOU, A. C., GREGORIOU, G., BLETSAS, A., DIMITRIOU, A., SAHALOS, J. A UHF radio frequency identification (RFID) system for healthcare: design and implementation. *International ICST Conference on Wireless Mobile Communication and Healthcare* (*2010 MOBIHEALTH*). Ayia Napa (Cyprus), 2010.

[7] SAUNDERS, S. R. *Antennas and Propagation for Wireless Communication Systems*. New York: Wiley, 1999.

[8] BALANIS, C. A. *Advanced Engineering Electromagnetics*. Chapter 5.5.2.D, p. 235—236. New York: Wiley, 1989.

[9] LANDRON, O., FEURSTEIN, M. J., RAPPAPORT, T. S. A comparison of theoretical and empirical reflection coefficients for typical exterior wall surfaces in a mobile radio environment. *IEEE Transactions on Antennas and Propagation*, 1996, vol. 44, no. 3, p. 341 - 351.

[10] OESTGES, C., CLERCKX B., RAYNAUD, L., VANHOENACKER-JANVIER, D. Deterministic channel modeling and performance simulation of microcellular wide-band communication systems. *IEEE Transactions on Vehicular Technology*, 2002, vol. 51, no. 6, p. 1422 - 1430.

[11] CUTY, J-P., DECLERCQ, M., DEHOLLAIN, C., JOEHL, N. *Design and Optimization of Passive UHF RFID Systems*. Berlin: Springer, 2007.

[12] BLETSAS, A., DIMITRIOU, A. G., SAHALOS J. N. Improving backscatter radio tag efficiency. *IEEE Transactions on Microwave Theory and Techniques*, 2010, vol. 58, no 6, p. 1502 - 1509.

[13] NIKITIN, P. V., RAO, K. V. S., MARTINEZ, R., LAM, S. F. Sensitivity and impedance measurements of UHF RFID chips. *IEEE Transactions on Microwave Theory & Techniques*, 2009, vol. 57, no. 5, part 2, p. 1297 - 1302.

[14] NXP, *UCODE G2XM and UCODE G2XL, data sheet*. Eindhoven (The Netherlands).

[15] Impinj, *IPJ-P5002-D2, data sheet*. Seattle (USA).

[16] Allien, *Higgs-3, data sheet*. Morgan Hill (CA, USA).

[17] GRIFFIN, J. D., DURGIN, G. D., HALDI, A., KIPPELEN, B. RF tag antenna performance on various materials using radio link budgets. *IEEE Antennas & Wireless Propagation Letters*, 2006, vol. 5, no. 1, p. 247 - 250.

[18] Alien, *ALN-9662 Squiggle-SH Inlay, data sheet.* Morgan Hill (CA, USA).

[19] INSTOCK Wireless Components Inc. *PD1020 - Two-Way Power Divide, 0.7-2.7 GHz, 40 Watts, data sheet*. New Jersey (USA).

[20] MTI Wireless Edge Ltd. *MT-242017/NRH, MT-242032/NRH, data sheet.* Israel.

[21] Andrew Corporation, *LDF1-50 Coaxial Cable*, *data sheet*. USA.

About Authors ...

Antonis G. DIMITRIOU received the diploma and the Ph.D degree in Electrical and Computer Engineering from the Aristotle University of Thessaloniki (AUTh), Greece, in 2001 and 2006, respectively. Since 2007, he is with the department of Electrical & Computer Engineering of AUTh. He has participated in 16 research projects in the fields of communications, antennas, propagation, signal processing and RFIDs. He is the author or co-author of approximately 30 journal and conference papers. His current interests are in the areas of EM-wave propagation, optimization of wireless networks, relay techniques in wireless communications, sensors and RFIDs.

Aggelos BLETSAS received with excellence his diploma degree in Electrical and Computer Engineering from Aristotle University of Thessaloniki, Greece in 1998, and the S.M. and Ph.D. degrees from Massachusetts Institute of Technology in 2001 and 2005, respectively. He worked at Mitsubishi Electric Research Laboratories (MERL), Cambridge MA, as a Postdoctoral Fellow and at Radiocommunications Laboratory (RCL), Department of Physics, Aristotle University of Thessaloniki, as a visiting scientist. He joined Electronic and Computer Engineering

Department, Technical University of Crete, in summer of 2009, as an Assistant Professor. His research interests focus on scalable wireless communication and networking.

Anastasis C. POLYCARPOU is a Professor at the University of Nicosia in the Department of Electrical & Computer Engineering. He graduated from Arizona State University in 1992 earning a BSEE degree in Electrical Engineering (EE) with Summa Cum Laude. He continued his graduate studies at the same university where he received an MS degree in EE in 1994 and a PhD degree in 1998. He has an extensive experience in funded research projects related to antenna analysis and design, microwave circuits and high-frequency electronic packaging, numerical methods in Electromagnetics, mode-matching and analytical methods, and radio frequency identification (RFID). He is a Senior Member of IEEE and a reviewer of scientific articles published in PIERS, JEMWA, IEEE, and IET magazines.

John N. SAHALOS received his B.Sc. degree and Ph.D in Physics. He also received the Diploma (BCE+MCE) in Civil Engineering and the professional Diploma of postgraduate studies in Radio-Electrology. He worked at the ElectroScience Laboratory, the Ohio State University, Columbus, as a Postdoctoral University Fellow. He was a Professor at the University of Thrace and a Professor at the AUTH. Dr. Sahalos is now Professor at the ECE Department of the University of Nicosia, Cyprus and director of the Radio & Telecommunications Laboratory (RTeLab). He was a visiting Professor at several Universities in USA and Europe. He is the author of four books (three of them in Greek), seven book chapters and more than 400 articles published in the scientific literature.